IET Power Electronics

Research Article

IET Journals
The Institution of Engineering and Technology

Design methodology of high performance domestic induction heating systems under worktop

ISSN 1755-4535
Received on 13th June 2019
Revised 11th October 2019
Accepted on 23rd October 2019
E-First on 20th November 2019
doi: 10.1049/iet-pel.2019.0693
www.ietdl.org

Emilio Plumed[1] ✉, Jesús Acero[1], Ignacio Lope[2], José M. Burdío[1]

[1]*Department of Electronic Engineering and Communications, I3A, Universidad de Zaragoza Maria de Luna 1, 50018 Zaragoza, Spain*
[2]*BSH Electrodomésticos España S.A., Avenida de la Industria 49, 50016 Zaragoza, Spain*
✉ *E-mail: eplumed@unizar.es*

Abstract: This study presents design guidelines for planar induction systems whose winding is considerably farther from its load than in usual arrangements. Optimum efficiency design is paramount for larger distances due to the magnetic field dispersion. To this end, a parameterised finite element model is used to ascertain the system's parameters in this new configuration. This model is used to test variations in frequency, inductor-load distance and inductor diameter. From simulation results, efficiency, output power, power loss volumetric density and near field measurement predictions are obtained. Graphical representation of these results is used to determine the viability of each possible design, choosing one to develop a prototype. Moreover, a study was carried out with Pareto techniques to determine the effect of ferrite coverage and thickness, as well as its distance to the aluminium shielding on efficiency and near field predictions in order to develop a second prototype. The validity of the model is confirmed by experimental tests in small and operating signal regimes.

1 Introduction

Induction cooktops contain planar windings over which a vessel is placed at a small distance, in order to transfer power. A medium frequency (between 20 and 100 kHz) alternating current is driven through the inductor, which induces losses in the vessel due to two phenomena, Joule effect dissipation of induced currents and magnetic hysteresis in the ferromagnetic material. The distance between inductor and vessel is in most cases determined by the thickness of both ceramic glass and electric insulation materials. This distance varies from 4 to 6 mm in current applications, as depicted in Fig. 1, which allows achieving high energy transfer efficiency and low magnetic field emissions [1]. However, the advent of new technologies and kitchen market trends push towards increasing this distance, such as the integration of induction cooktops beneath kitchen worktops, as shown in Fig. 2. This change will mean a significant modification of specifications that will require redesigning current inductors. As an example, a commercial 180 mm diameter inductor has been simulated, and its efficiency and volumetric loss density versus distance are shown in Fig. 3.

Considering that coupling between magnetic elements decreases when the distance between them increases [2], energy transfer becomes less and less efficient. This study presents an inductor design method to operate at a distance from vessels greater than 5 mm and achieving the best possible performance and efficiency. Inductor-load distance will not necessarily be a fixed input parameter; rather the design objective could be to reach a compromise between distance and efficiency.

Fig. 1 *Typical induction heating system*

Since a long distance between inductor and load has rarely been needed in the past, previous work barely focused on it [3]. Therefore, this study seeks to use existing methods for magnetic modelling [4–8] and losses calculations [9–18] and apply them to this new configuration. Additionally, the B field was carefully studied to check for norm compliance [19–22], and several topologies were considered for the prototype's construction [23–28].

This paper is organised as follows. In Section 2, both the simulation model and the optimisation process are introduced. Section 3 shows simulation results. Section 4 analyses the effect of ferrite coverage and aluminium tray proximity on efficiency and near field measurement predictions, as well as providing further design considerations. Section 5 presents the prototypes and experimental verification of the calculations. Section 6 reports the conclusions drawn from this study.

2 Inductor-load system model

2.1 Geometry and simulation parameter definition

Maxwell's equations [4] are solved for each geometry by means of a finite element model to analyse their influence on inductor-load system parameters. A 2D axisymmetric geometry as depicted in Fig. 4 is considered in order to avoid long simulation times. Induction cooktops heat up ferromagnetic vessels across elements whose electromagnetic properties are similar to air; therefore they are not represented in this simulation. Inductor windings usually consist of twisted multi-stranded wires with litz structure (litz wires), allowing to consider equivalence between strands. Ferrite bars are placed beneath the inductor to conduct the magnetic field and also, to a lesser degree, shield the components below. The last element is an aluminium tray which completely shields magnetic fields and protects electronic components that are usually placed below.

At first, it is more useful to learn overall tendencies and trends in data instead of focusing on specific cases, so the simulated geometry is simplified. The inductor is modelled as a lossless and ideal current density, while its actual losses are computed by means of formulas, using the H field solution of the finite element analysis. The usual ferrite bars are replaced by a lossless magnetic disk with equivalent permeability and the aluminium tray is

removed in a first approach. The vessel is portrayed as a ferromagnetic cylinder [5] whose surface is assigned an impedance boundary condition. The model is simulated by COMSOL at different frequencies, using Matlab's Livelink to change its geometry, sweeping inductor diameters and inductor-load distances.

A sinusoidal current, I, of 1 ampere is driven through the inductor. The system's equivalent impedance seen from the inductor, Z_{ind}, is calculated from the voltage, V_{ind}, induced in the winding

$$V_{\text{ind}} = -\oint E_{\phi} \mathrm{d}l, \tag{1}$$

$$Z_{\text{ind}} = V_{\text{ind}}/I, \tag{2}$$

where E_{ϕ} is the electric field's azimuthal component. Z_{ind} is complex-valued, and can be broken down into its real and imaginary components

$$Z_{\text{ind}} = R_{\text{ind}} + \mathrm{j}\omega L_{\text{ind}}, \tag{3}$$

$$R_{\text{ind}} = R_{\text{load}} + R_{\text{al}}, \tag{4}$$

$$R_{\text{eq}} = R_{\text{load}} + R_{\text{al}} + R_{\text{w}}, \tag{5}$$

where R_{ind} is the induction resistance, R_{eq} is the system's total equivalent resistance and L_{ind} its equivalent inductance. R_{eq} can also be broken down into: R_{load} the vessel's resistance, R_{al} the aluminium tray's resistance and R_{w}, the copper winding losses that are computed analytically [9, 10].

R_{load} and R_{al} represent the power dissipated in the load and aluminium tray, respectively. Therefore, their contribution to the equivalent resistance can be computed from the power delivered to each element, which in turn is calculated by integrating the flux of Poynting's vector, $\boldsymbol{S}$, over their surface. $\boldsymbol{S}$ represents power surface density akin to $\boldsymbol{B}$ representing magnetic flux surface density

$$\boldsymbol{S} = \boldsymbol{E} \times \boldsymbol{H}^{*}, \tag{6}$$

$$P = \int_{S} \boldsymbol{S} \mathrm{d}S, \tag{7}$$

$$R = 2P/I^{2}, \tag{8}$$

where $\boldsymbol{E}$ is the electric field and $\boldsymbol{H}^{*}$ is the complex conjugate of the magnetic field.

Copper winding losses [11–13] are categorised into those caused by conduction: dc and skin effect, R_{cond}, and those caused by the magnetic field's proximity effect, R_{prox}, whose expressions for circular windings in 2D geometry are

$$R_{\text{w}} = R_{\text{cond}} + R_{\text{prox}}, \tag{9}$$

$$R_{\text{cond}} = \frac{n}{n_{\text{s}}} \frac{\pi(r_{\text{ext}} + r_{\text{int}})}{\pi r_{\text{s}}^{2} \sigma} \phi_{\text{cond}}(r_{\text{s}}/\delta), \tag{10}$$

$$R_{\text{prox}} = n^{3} n_{\text{s}} \frac{4\pi}{\sigma} \phi_{\text{prox}}(r_{\text{s}}/\delta) \left\langle 2\pi r \left| \bar{\boldsymbol{H}}_{\text{s},1} \right|^{2} \right\rangle, \tag{11}$$

where n is the winding's turn number, n_{s} the strand number, r_{ext} and r_{int} the inductor's external and internal radii, respectively, r_{s} the strand radius, σ the copper electric conductivity, $\overline{\boldsymbol{H}}_{\text{s},1}$ the magnetic field over the strands created by a single turn per current unit, ϕ_{cond} and ϕ_{prox} each a group of Bessel functions [15] representing the losses' dependence to r_{s} and copper skin depth, δ

$$\delta = \sqrt{\frac{1}{\pi \mu_{0} f \sigma}}, \tag{12}$$

where μ_{0} is the air's magnetic permeability and f is the frequency.

The resistances and inductance that contribute to the equivalent impedance can be related to those of an inductor of the same geometry but with a single turn and a single strand [29]

$$R_{\text{load}}/R_{\text{load},11} = R_{\text{al}}/R_{\text{al},11} = L_{\text{eq}}/L_{\text{eq},11} = n^{2}, \tag{13}$$

$$R_{\text{cond}}/R_{\text{cond},11} = n/n_{\text{s}}, \tag{14}$$

$$R_{\text{prox}}/R_{\text{prox},11} = n^{3} n_{\text{s}}, \tag{15}$$

where the subscript 11 marks the parameters of an ideal inductor with a single turn and a single strand. These relations allow the designer to simulate the behaviour of inductors of any number of turns and strands for a given geometry, which in turn allows for simpler, broader studies to analyse trends and develop guidelines.

2.2 Parameter optimisation

Inductor design is ruled by four criteria in this analysis: first, the desired rated power must be achieved when the power inverter works at resonance; second, a high efficiency must be achieved; third, heat dissipated by the inductor must be under a certain limit to avoid damaging cable isolation and connectors; fourth, magnetic

Fig. 2 *Induction cooktop integrated under the worktop*

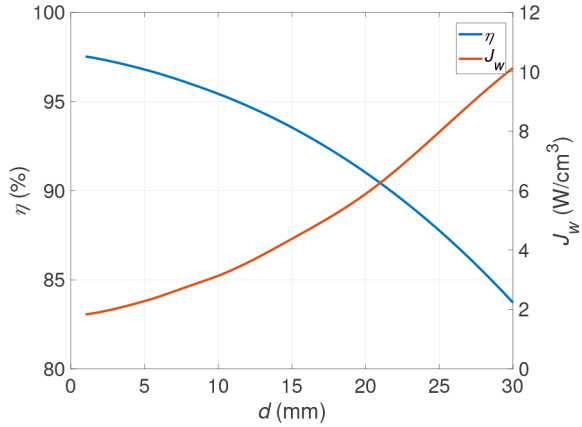

Fig. 3 *Efficiency versus distance of a commercial 180 mm diameter inductor*

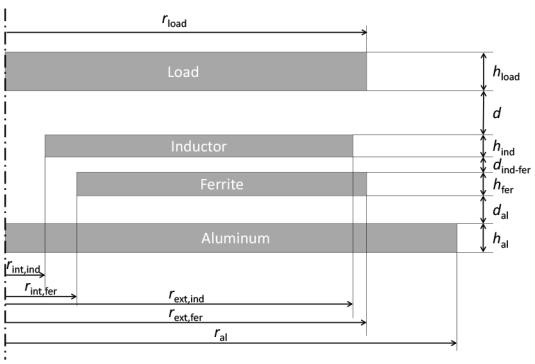

Fig. 4 *2D simulation geometry diagram*

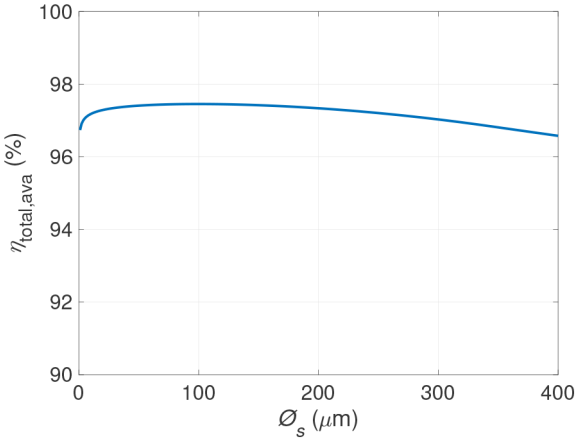

Fig. 5 *Conventional inductor efficiency (%) varying its strand diameter, $\varnothing_s$*

flux radiated must be under a certain value to be norm compliant [19–22].

Output power at the resonant frequency due to the first harmonic is

$$P_{\text{o,res}} = V_{1,\text{rms}}^2/\left(n^2 R_{\text{eq},11}\right), \tag{16}$$

where $V_{1,\text{rms}}$ is the root mean square value of the voltage's first harmonic feeding the inductor. Therefore, power can be adjusted by changing the number of turns.

The complete system's efficiency can be expressed as [7]

$$\eta_{\text{total}} = \frac{R_{\text{load}}}{R_{\text{load}} + R_{\text{al}} + R_{\text{cond}} + R_{\text{prox}}}. \tag{17}$$

The system's efficiency can be expressed in terms of the resistances of one strand and one turn inductors, becoming

$$\eta_{\text{total}} = \frac{R_{\text{load},11}}{R_{\text{load},11} + R_{\text{al},11} + R_{\text{cond},11}/nn_{\text{s}} + nn_{\text{s}}R_{\text{prox},11}}, \tag{18}$$

where the product between the number of strands and turns, nn_{s}, is proportional to the copper volume.

The inductor's total copper volume, V_{cu}, can be calculated from nn_{s}, r_{s}, and the mean turn length, l_{mean}, whose expressions for circular windings are

$$l_{\text{mean}} = \pi(r_{\text{int}} + r_{\text{ext}}), \tag{19}$$

$$V_{\text{cu}} = nn_{\text{s}}\pi r_{\text{s}}^2 l_{\text{mean}}. \tag{20}$$

In order to determine the optimum copper volume, the derivative with respect to nn_{s} is calculated as

$$\frac{\partial \eta_{\text{total}}}{\partial nn_s} = \frac{R_{\text{load},11}\left(R_{\text{cond},11}/nn_{\text{s}} - R_{\text{prox},11}\right)}{\left(R_{\text{load},11} + R_{\text{al},11} + R_{\text{cond},11}/nn_{\text{s}} + R_{\text{prox},11}\right)^2}. \tag{21}$$

Hence, maximum efficiency versus nn_{s} [16, 17] happens when

$$nn_{\text{s,ideal}} = \sqrt{R_{\text{cond},11}/R_{\text{prox},11}}. \tag{22}$$

However, the ideal copper volume is usually bigger than the available winding's volume for each inductor geometry, so the maximum copper volume must also be taken into account

$$nn_{\text{s,max}} = K_{\text{u}}\frac{h_{\text{ind}}(r_{\text{ext}} - r_{\text{int}})}{\pi r_{\text{s}}^2}, \tag{23}$$

where K_{u} is the packing factor, which is the ratio between copper volume in the inductor and its total volume and h_{ind} is the inductor's thickness. Owing to the strands' insulation, K_{u} decreases when r_{s} is reduced [18]. The available copper volume, $nn_{\text{s,ava}}$, is defined as the optimum volume limited by its maximum. Consequently, the available efficiency can be derived as the one achieved with the available copper volume

$$\eta_{\text{total,ava}} = \frac{R_{\text{load},11}}{R_{\text{load},11} + R_{\text{al},11} + R_{\text{cond},11}/nn_{\text{s,ava}} + nn_{\text{s,ava}}R_{\text{prox},11}}. \tag{24}$$

Copper power losses, P_{w}, are calculated as the difference between total and effective power

$$P_{\text{cu}} = (1 - \eta_{\text{cu,ava}})P_{\text{o}}, \tag{25}$$

where copper efficiency, η_{cu}, is defined as

$$\eta_{\text{cu}} = \frac{R_{\text{load}}}{R_{\text{load}} + R_{\text{cond}} + R_{\text{prox}}}. \tag{26}$$

Therefore, copper power loss density, J_{cu}, is

$$J_{\text{cu}} = P_{\text{cu}}/V_{\text{cu}}, \tag{27}$$

where V_{cu} is the copper volume from (20).

Near field emission measurements are taken with a spherical probe that houses three perpendicular, circular loops of wire of 100 cm^2 surface area. For induction cooktops, in particular, the probe is placed 30 cm from the appliance's edge. Since the inductor position can vary greatly with the cooktop's layout, in the FEA tool the simulated probe is placed 30 cm away from the inductor's edge for a worst case scenario. The three probe loops are aligned with the simulation axes. The measurement value is the norm of the field averages in each loop

$$B_{\text{ax},i,\text{mean}} = \frac{1}{S_{100}}\int_{S_i} B_{\text{ax},i}\text{d}S_i, \tag{28}$$

$$B_{\text{norm}} = \sqrt{B_{\text{ax},1,\text{mean}}^2 + B_{\text{ax},2,\text{mean}}^2 + B_{\text{ax},3,\text{mean}}^2}, \tag{29}$$

where S_{100} is the area of each loop, the subscript mean denotes that the values are averaged and ax, i represents the generic ith directional vector of coordinate system ax. For cylindrical coordinates, they become r, ϕ, z, and x, y, z for Cartesian.

Magnetic flux density is proportional to the turn number and inductor current, so its value can be obtained from a simulation with one turn and one ampere

$$B_{\text{norm}} = nIB_{\text{norm},11}. \tag{30}$$

3 Simulation results

3.1 Trend analysis

The influence of design variables on goal parameters is shown below. As seen in the previous section, strand radius, r_{s}, affects losses and available copper volume, reaching more desirable results by decreasing r_{s}. In spite of that, for small strand diameters, insulation thickness becomes more relevant, reducing the packing factor, K_{u}. This reduction also diminishes the maximum copper volume, which in turn decreases efficiency, as shown in Fig. 5.

Working at frequencies lower than 60 kHz, which is most of the time for induction cooktops, the copper optimum volume is higher than the maximum, so in most cases filling the inductor's housing with copper provides the best design.

Fig. 6 shows that available efficiency increases with inductor diameter and decreases when load distance increases. This is mainly due to the variation in the magnetic coupling between inductor and load. There is a bigger coupling for smaller distances or bigger diameters. Moreover, with bigger diameters, the effect of the distance is noticeably reduced.

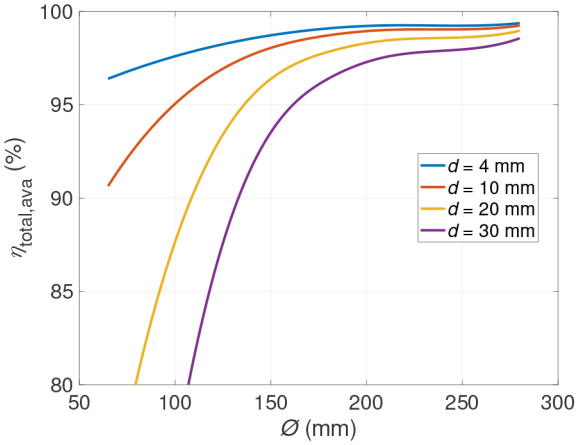

Fig. 6 *Total available efficiency (%) sweeping inductor diameter for several inductor–load distances at 30 kHz*

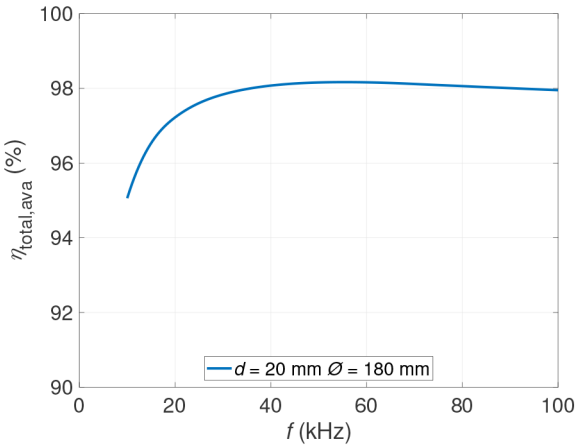

Fig. 7 *Total available efficiency (%) sweeping frequency in a 180 mm inductor working at a 20 mm distance*

Fig. 7 shows the total available efficiency depending on frequency. At low frequencies, the available copper volume is much lower than its optimum, so efficiency is reduced, while at high frequencies, having reached optimum copper volume, conduction and proximity losses keep increasing, so an efficiency maximum is reached at an intermediate frequency. An inductor efficiency higher than 96% should be achieved in order to keep up with current designs that work at 4 mm.

Copper power loss density follows the same trend as efficiency, except that as inductor diameter increases, so does its volume, thus power loss density decreases even faster, as shown in Fig. 8. In order to avoid overheating problems in inductors, J_w should be kept below a certain limit, which can vary anywhere between 4 and 6 W/cm^3 depending on the cooktop's layout, cooling mechanism, size, and so on.

Near field emissions simulated as per norm are shown in Fig. 9. They increase with inductor–load distance, while they decrease when inductor diameter increases at equal power rating. However, smaller inductors have reduced power ratings, so below 200 mm, near field measurements can go up and down. A lower magnetic coupling causes an outward 'leak' of magnetic flux. The magnetic field weakens with frequency increments, so its measurement also diminishes. The magnetic flux density limit imposed by the norm between 800 Hz and 150 kHz is 6.25 µT, so in cases where results are higher than this value, additional measurements must be taken to mitigate it.

4 Further design analysis and considerations

As mentioned in the conclusions of [30], a thorough analysis of ferrite quantity was called for to determine its effects on efficiency and radiated near field. Therefore, a 3D simulation was carried out to sweep the ferrite coverage, ferrite thickness, h_{fer}, and ferrite–

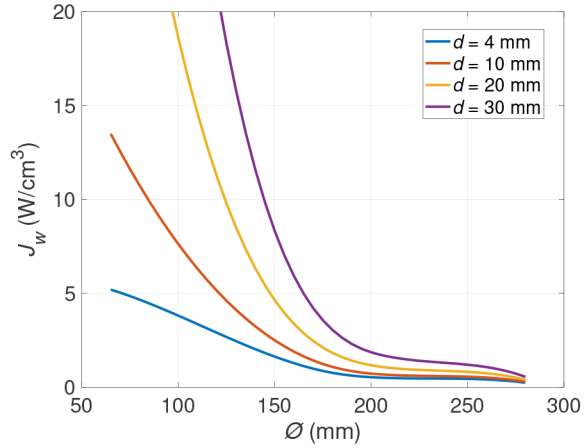

Fig. 8 *Loss power density (W/cm^3) sweeping inductor–load distance and inductor diameter at 30 kHz*

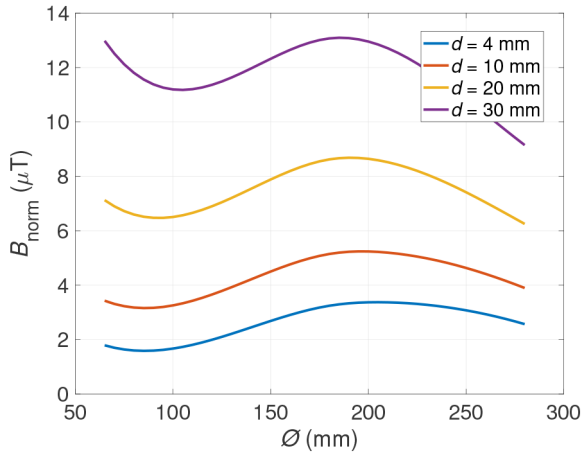

Fig. 9 *Magnetic flux density (µT) measured 30 cm from the inductor's edge, sweeping inductor diameter for several inductor–load distances at 30 kHz*

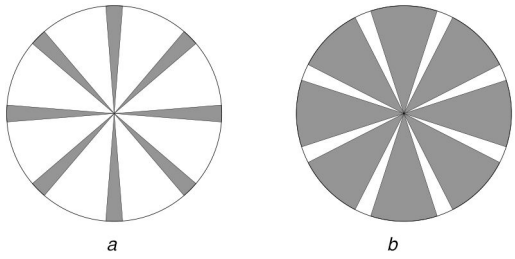

Fig. 10 *Coverage examples of* ***(a)*** 20%, ***(b)*** 80%

aluminium distance, d_{fer-al}, in order to design a 210 mm diameter inductor to work at a 34 mm distance. In this case, ferrite coverage is modified using eight circular sectors of a variable central angle, from 0° (0% coverage) to 360°/8 (100% coverage), as indicated in Fig. 10.

The effect on the efficiency is measured with the power loss density, J_w, in order to consider both the thermal and electromagnetic limits. The resulting loss density and near field estimation are represented in Fig. 11 to determine Pareto efficiency [31], with marker shape indicating ferrite thickness, marker colour representing ferrite–aluminium distance and line greyscale representing ferrite coverage.

Ferrite coverage produces the most noticeable decrease in losses, as well as a small increment in near field emissions. An increase in either ferrite thickness or ferrite–aluminium distance significantly boosts near field emissions while decreasing J_w at a reduced rate the bigger the distance becomes. In fact, the effect of ferrite thickness is mostly related to the implicit change in distance

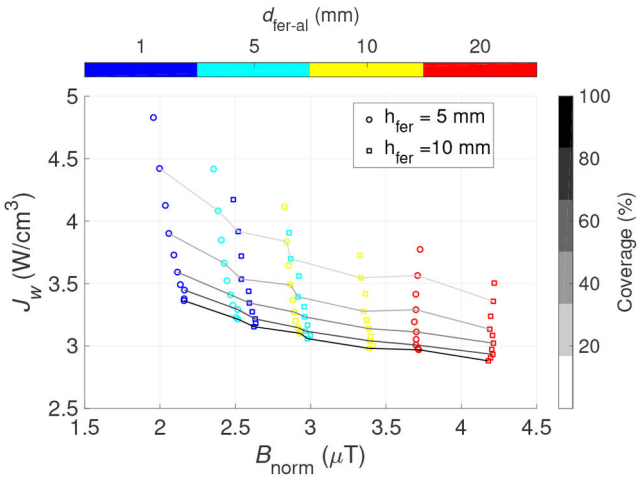

Fig. 11 *Power loss density versus near field of simulated cases*

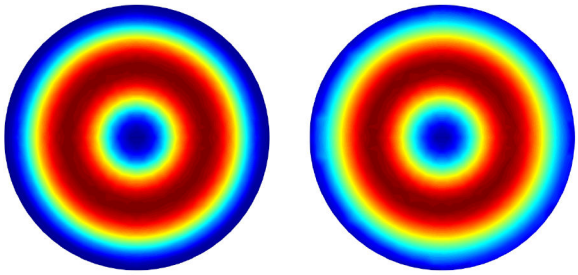

Fig. 12 *Power distribution at* ***(a)*** 4 mm, ***(b)*** 34 mm

Fig. 13 *Prototype inductors of* ***(a)*** 180 mm diameter, ***(b)*** 210 mm diameter

to the aluminium, as can be seen in Fig. 11, for the 5 mm distance, 10 mm thickness points in relation to their reciprocal 10 mm distance, 5 mm thickness points, which are very close together.

Although increasing ferrite coverage is mostly beneficial, ferrite quantity also increases weight and cost, so all involved input parameters have positive and negative effects. Aside from the cases with the highest J_w, there is no design that is superior in every circumstance, making each individual application determine the balance it needs between losses, near field emissions, and ferrite quantity. In the case of this study, the most important criteria were to minimise overall appliance height and minimise J_w, so the smallest aluminium distance and ferrite thickness were chosen, as well as a ferrite coverage of 100% using a ferrite plane. The second inductor prototype was designed following these guidelines.

In order to qualitatively determine the thermal performance of the system, the surface power density has been represented via Poynting's vector, $\boldsymbol{S}$, in Fig. 12 comparing the results at 4 and 34 mm distances. As can be seen, both distributions are very similar. The annulus with the highest power density, represented by its dark red colour, is slightly wider for 4 mm, but low power zones represented by their bright blue colour extend a bit further in the 34 mm case. The temperature distribution is usually an averaged and blurred version of the power distribution, so despite these minor differences, the thermal performance is expected to be nearly identical to conventional induction heating.

The interference of inductors working in close proximity is a plausible drawback of this system. Therefore, a simulation was carried out where two identical inductors are placed within 10 mm of each other, placing a vessel on top of one of them and obtaining their impedances. When the vessel is at a 4 mm distance, the inductive coupling coefficient, k, between inductors is 0.0053, while at 34 mm k becomes 0.0174, more than triple. Nevertheless, k is still very low, so in appliances where each inductor would heat its own individual load, the mutual interference can probably be neglected.

5 Experimental verification

5.1 Inductor design

A medium-sized inductor was considered for a first prototype. This prototype inductor should work at the longest possible distance while maintaining good performance parameters. Fig. 7 shows that a good efficiency can be reached for a 180 mm inductor working at 20 mm distance and 40 kHz. Considering that in this case the near field limit is exceeded, it will be necessary to mitigate it by additional measures.

For inductors with continuous turns, such as the one shown in Fig. 13*a*, the maximum number of strands of 0.2 mm in diameter is around 3400. A power rating of 3000 W can be reached at 40 kHz with 19 turns, so the litz wire can have up to 180 strands. Instead of using a ferrite plane, the inductor has five rectangular ferrite bars in addition to an aluminium tray. These modifications from previous simulations will alter the system's equivalent impedance, so this new configuration has been simulated in 3D.

Additionally, after the initial results presented in [30], a second inductor prototype of 210 mm diameter, shown in Fig. 13*b* was designed, with the results from the previous section, to work at a distance of 34 mm delivering 3700 W. The maximum number of strands, in this case, is close to 4200, so the needed 29 turns were wound with 144 strands wire.

5.2 Simulation verification

In order to substantiate the simulation's results, the real prototype geometry has been studied by means of a three-dimensional simulation. The prototype in Fig. 13*a* has been measured at small and real signal regimes, using an impedance analyser, and transmitting power to a ferromagnetic vessel, respectively. The prototype in Fig. 13*b* has been measured at the real signal regime only.

The first inductor has been measured without load with an LCR meter, obtaining resistance and inductance data represented in Fig. 14, where the continuous line represents the simulated data and the dots represent the measured data.

These simulated resistance values are nearly spot-on, while the inductance has a very small error at all frequencies as well as a bigger error at very high frequencies due to the self-resonance effects not considered in the simulation.

Induction cooktops can use a wide variety of inverters [23–25] to power the system. In this case, a half-bridge inverter was used for its reduced number of components and degrees of freedom [26, 27]. Real signal data has been obtained with the setup shown in Fig. 15 at a 0.5 duty cycle while sweeping frequencies in order to vary output power. Delivered power and current results are shown in Fig. 16 for both prototypes, with simulated data represented by continuous lines and measured data by dots.

Since both electronics and resonant capacitors are rated to work at 40 A, power has not been increased beyond that point for safety's sake. Measurements show agreement with simulated data for the considered power range.

A field probe was also used to measure the magnetic flux density near the system in order to verify the simulated values. For this measurement, the oscilloscope probes were removed and the aluminium tray with the inductor was put back in their casing, shown in the background of Fig. 15. Fig. 17 shows the values taken at 3100 W at several points of increasing distance. The figure

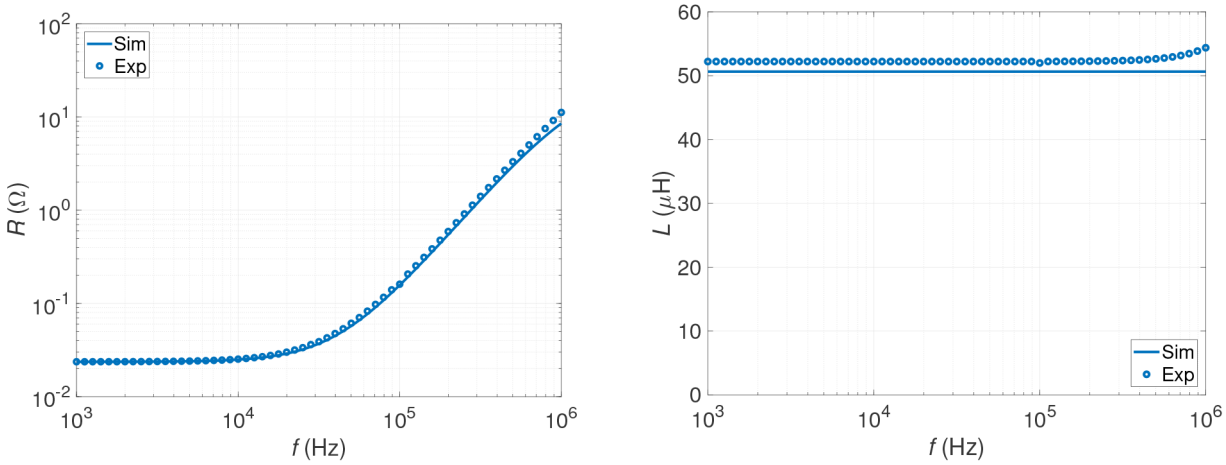

a b

Fig. 14 *Prototype inductor LCR results, where the continuous line shows simulated values and the dots represent measured values*
(a) Equivalent resistance, ***(b)*** Equivalent inductance in the air

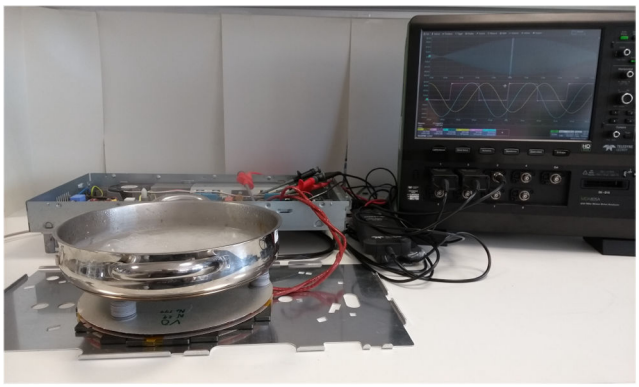

Fig. 15 *Power measurement setup*

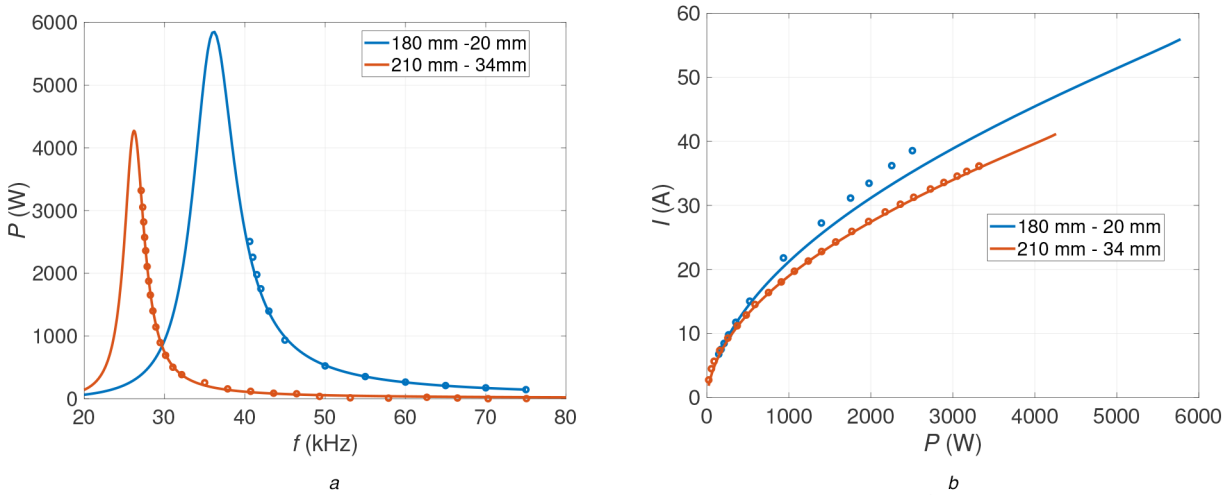

a b

Fig. 16 *Experimental results at the real signal regime for the 180 mm prototype and the 210 mm prototype.*
(a) Output power, ***(b)*** Inductor current

shows that the simulation becomes more accurate the farther the probe is to the system, which is fortunate because the norm measurements are taken at 30 cm. It is also worth noting that the simplified simulation geometry does not take into account the appliance's metal casing, which is the likeliest cause of the reduced field measurements compared with the simulated values.

6 Conclusions

All in all, domestic induction heating is possible at higher distances, considering a careful design and mindfulness of the existing limitations.

Since winding losses are not a limiting factor for inductors the same size as the prototype or bigger, total efficiency is a suitable indicator of good design.

Based on that, smaller inductors can work at a 20 or 25 mm distance at most. In order to work across larger gaps, it is necessary to use bigger inductors or consider other options, such as wireless energy transfer with multiple inductors.

Ferrite coverage has a significant impact on inductor efficiency, so it must be taken into account in the design process. If there is enough space for it and near field emissions are well below norm limits, distancing the aluminium tray can provide a small and easy efficiency boost.

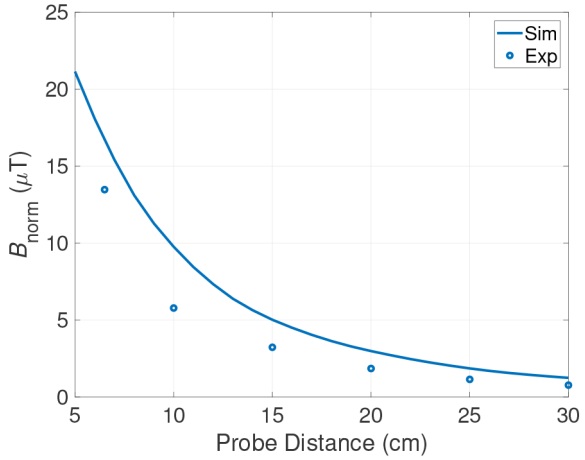

Fig. 17 *B_{norm} measured at different distances*

Thermal distribution is barely affected by the distance increase.

Interference between inductors in close proximity can be neglected if they heat different vessels.

Based on our B-field measurement, careful casing design could also help reduce near field emissions.

The experimental measurements carried out to agree with the model's results, so simulation data can be trusted.

7 Acknowledgments

This work was partly supported by the Spanish MINECO under Project TEC2016-78358-R, by the Spanish MICINN and AEI under Project RTC-2017-5965-6, co-funded by EU through FEDER program, by the BSH Home Appliances Group and by the Gobierno de Aragón-FSE 2014-20 under grant IIU/2023/2017.

8 References

[1] Lucía, O., Maussion, P., Dede, E.J., *et al.*: 'Induction heating technology and its applications: past developments, current technology, and future challenges', *IEEE Trans. Ind. Electron.*, 2014, **61**, (5), pp. 2509–2520

[2] Davies, J., Simpson, P.: '*Induction heating handbook*' (McGraw-Hill Companies, USA, 1979)

[3] Acero, J., Lucía, O., Carretero, C., *et al.*: 'Efficiency improvement of domestic induction appliances using variable inductor-load distance'. Proc. 27th Annual IEEE Applied Power Electronics Conf. and Exposition (APEC), Orlando, FL, USA, 2012, pp. 2153–2158

[4] Stratton, J.: '*Electromagnetic theory*' (McGraw-Hill, New York, 1941)

[5] Acero, J., Lucia, O., Millan, I., *et al.*: 'Identification of the material properties used in domestic induction heating appliances for system-level simulation and design purposes'. Applied Power Electronics Conf. and Exposition (APEC), 2010 25th Annual IEEE, Palm Springs, CA, USA, 2010, pp. 439–443

[6] Meng, L.C., Cheng, K.W.E., Chan, K.W., *et al.*: 'Variable turn pitch coils design for heating performance enhancement of commercial induction cooker', *IET Power Electron.*, 2012, **5**, (1), pp. 134–141

[7] Serrano, J., Acero, J., Lope, I., *et al.*: 'A flexible cooking zone composed of partially overlapped inductors', *IEEE Trans. Ind. Electron.*, 2018, **65**, (10), pp. 7762–7771

[8] Carretero, C., Lucia, O., Acero, J., *et al.*: 'Frequency-dependent modelling of domestic induction heating systems using numerical methods for accurate time-domain simulation', *IET Power Electron.*, 2012, **5**, (8), pp. 1291–1297

[9] Hernandez, P., Monterde, F., Burdio, J.M., *et al.*: 'Power losses distribution in the litz-wire winding of an inductor for an induction cooking appliance'. Proc. IEEE 2002 28th Annual Conf. Industrial Electronics Society (IECON'02), Seville, Spain, 2002, vol. 2, pp. 1134–1137

[10] Wojda, R.P., Kazimierczuk, M.K.: 'Winding resistance of litz-wire and multi-strand inductors', *IET Power Electron.*, 2012, **5**, (2), pp. 257–268

[11] Acero, J., Alonso, R., Burdio, J.M., *et al.*: 'A model of losses in twisted-multistranded wires for planar windings used in domestic induction heating appliances'. Proc. APEC 07 – 22nd Annual IEEE Applied Power Electronics Conf. and Exposition, Anaheim, CA, USA, 2007, pp. 1247–1253

[12] Ferreira, J.A.: 'Analytical computation of AC resistance of round and rectangular litz wire windings', *IEE Proc. B, Electr. Power Appl.*, 1992, **139**, (1), pp. 21–25

[13] Deng, Q., Liu, J., Czarkowski, D., *et al.*: 'Frequency-dependent resistance of litz-wire square solenoid coils and quality factor optimization for wireless power transfer', *IEEE Trans. Ind. Electron.*, 2016, **63**, (5), pp. 2825–2837

[14] Roßkopf, A., Bär, E., Joffe, C.: 'Influence of inner skin- and proximity effects on conduction in litz wires', *IEEE Trans. Power Electron.*, 2014, **29**, (10), pp. 5454–5461

[15] Carretero, C.: 'Coupling power losses in inductive power transfer systems with litz-wire coils', *IEEE Trans. Ind. Electron.*, 2017, **64**, (6), pp. 4474–4482

[16] Acero, J., Hernandez, P.J., Burdio, J.M., *et al.*: 'Simple resistance calculation in litz-wire planar windings for induction cooking appliances', *IEEE Trans. Magn.*, 2005, **41**, (4), pp. 1280–1288

[17] Sullivan, C.R.: 'Optimal choice for number of strands in a litz-wire transformer winding', *IEEE Trans. Power Electron.*, 1999, **14**, (2), pp. 283–291

[18] Lope, I., Acero, J., Carretero, C.: 'Analysis and optimization of the efficiency of induction heating applications with litz-wire planar and solenoidal coils', *IEEE Trans. Power Electron.*, 2016, **31**, (7), pp. 5089–5101

[19] AENOR: 'UNE-EN 50366 Aparatos electrodomésticos y análogos. Campos electromagnéticos. Métodos de evaluación y medición.'

[20] Viellard, C., Romann, A., Lott, U., *et al.*: 'B-field exposure from induction cooking appliances'. 28th Annual Meeting Abstracts of the Bioelectromagnetics Society, Cancun, Mexico, 11–15 June 2006. Available at: https://www.bag.admin.ch/dam/bag/de/dokumente/str/nis/faktenblaetter-emf/b-field-exposure.pdf.download.pdf/B-Field%20Exposure%20From%20Induction%20Cooking%20Appliances%20-%20ITIS%202007.pdf

[21] Ahlbom, A., Bergqvist, U., Bernhardt, J., *et al.*: 'Guidelines for limiting exposure to time-varying electric, magnetic, and electromagnetic fields (up to 300 GHz)', *Health Phys.*, 1998, **74**, (4), pp. 494–521

[22] ICNIRP: 'Guidelines for limiting exposure to time-varying electric and magnetic fields (1 Hz to 100 kHz)', *Health Phys.*, 2010, **99**, (6), pp. 818–836

[23] Mohan, N., Undeland, T.M.: '*Power electronics: converters, applications, and design*' (John Wiley & Sons, USA, 2007)

[24] Lucia, O., Burdio, J.M., Millán, I., *et al.*: 'Efficiency-oriented design of ZVS half-bridge series resonant inverter with variable frequency duty cycle control', *IEEE Trans. Power Electron.*, 2010, **25**, (7), pp. 1671–1674

[25] Esteve, V., Jordán, J., Sanchis-Kilders, E., *et al.*: 'Enhanced pulse-density-modulated power control for high-frequency induction heating inverters', *IEEE Trans. Ind. Electron.*, 2015, **62**, (11), pp. 6905–6914

[26] Millán, I., Burdío, J.M., Acero, J., *et al.*: 'Series resonant inverter with selective harmonic operation applied to all-metal domestic induction heating', *IET Power Electron.*, 2011, **4**, (5), pp. 587–592

[27] Carretero, C., Lucia, O., Acero, J., *et al.*: 'Phase-shift modulation in double half-bridge inverter with common resonant capacitor for induction heating appliances', *IET Power Electron.*, 2015, **8**, (7), pp. 1128–1136

[28] Sarnago, H., Lucia, O., Mediano, A., *et al.*: 'High-efficiency parallel quasi-resonant current source inverter featuring SiC metal-oxide semiconductor field-effect transistors for induction heating systems with coupled inductors', *IET Power Electron.*, 2013, **6**, (1), pp. 183–191

[29] Acero, J., Carretero, C., Alonso, R., *et al.*: 'Quantitative evaluation of induction efficiency in domestic induction heating applications', *IEEE Trans. Magn.*, 2013, **49**, (4), pp. 1382–1389

[30] Plumed, E., Acero, J., Burdío, J.M., *et al.*: 'Design method for domestic induction heating systems with a larger load distance'. Proc. IECON 2017 – 43rd Annual Conf. IEEE Industrial Electronics Society, Beijing, People's Republic of China, 2017, pp. 3785–3790

[31] Bosshard, R., Kolar, J.W., Mühlethaler, J., *et al.*: 'Modeling and η-α-pareto optimization of inductive power transfer coils for electric vehicles', *IEEE J. Emerging Sel. Top. Power Electron.*, 2015, **3**, (1), pp. 50–64